Catal Lett (2007) 119:289–295
DOI 10.1007/s10562-007-9233-3

# Silver Nanoparticles in Mesoporous Aerogel Exhibiting Selective Catalytic Oxidation of Benzene in $CO_2$ Free Air

**K. Balkis Ameen · K. Rajasekar · T. Rajasekharan**

Received: 27 March 2007 / Accepted: 30 July 2007 / Published online: 15 August 2007


**Abstract** The present article reports the synthesis of silver nanoparticles in silica aerogel matrix by sub-critical drying technique. The catalytic performance of these nanocomposites was evaluated for the selective oxidation of benzene. Silica aerogel with 1, 5, 10 and 25 wt.% of silver was prepared and characterized for their physico-chemical characteristics. The catalytic performance of these samples was evaluated as a function of silver particle size crystallized within the aerogel matrix. The sample with the silver concentration of 1 wt.% showed high selectivity among the tested samples. With increasing silver particle size, the % conversion increased with a decreased selectivity, which is attributed to the particle size effect on the catalytic oxidation of benzene.

**Keywords** Silver nanoparticles · Silica aerogel · Sub-critical drying technique · Selective oxidation of benzene

## 1 Introduction

Aerogels are emerging materials in the field of catalysis, when compared to the ordered micro- and mesoporous materials [1, 2]. Aerogels have porosities up to 99.8% and a large surface area of 500–1200 $m^2\ g^{-1}$ made by supercritical drying method [3]. Such a large specific surface area offered by the aerogel matrix can be used to host finely dispersed metallic particles [4], which enables increased number of active sites per gram of the material. The cost involved in supercritical drying is a disadvantage and to circumvent this drawback, other alternate ambient pressure drying processes have been developed [5]. Sub-critical drying, one of the above said techniques is an economical processing route that can be used for the stabilization of nanoparticles in the silica aerogel matrix. Some of the chemical reactions reported with them are selective oxidation of iso-butylene using $NiO–Al_2O_3$, $NiO–SiO_2–Al_2O_3$ [6] and Fischer–Tropsch synthesis using $Fe_2O_3–SiO_2$ [7].

Selective oxidation of benzene to phenol is an industrially important chemical conversion. Shu-ichi Niwa has studied the above conversion with Pd dispersion [8] in porous alumina tube using oxygen; the process exhibited good selectivity but the yield was not promising. Photocatalysis using homogeneous (titania) and heterogeneous system (polyoxometalates) shows positive result for benzene oxidation [9]. Other systems using metal dispersed zeolites and heteropoly compounds have also been cited towards this conversion [10, 11].

The direct reaction of benzene with molecular oxygen requires either the presence of radical initiators [12] or transition metal oxide/phosphate catalysts [13]. Since these materials have MFI structure, the diffusion of products becomes difficult and to overcome this, it is imperative to select mesoporous materials. Introduction of Ti into V-MCM-41 solids has resulted in an increased activity in the oxidation of styrene and benzene [14]. Niobium and niobium-cobalt-containing mesoporous redox molecular sieves [15] showed a high activity towards styrene

K. Balkis Ameen · T. Rajasekharan
Defence Metallurgical Research Laboratory,
Hyderabad 500 058, India

K. Balkis Ameen (✉)
Vellore Institute of Technology, VIT, Vellore,
Tamilnadu 632014, India
e-mail: kbameen@yahoo.com

K. Rajasekar
Anna University, Chennai 600 025, India

oxidation and very low activity towards benzene oxidation with $H_2O_2$. The use of noble metals in the catalysis of oxidation reactions offers a wide variety of sites for the activation of clean oxidants such as molecular oxygen, hydrogen peroxide and nitrous oxide. Few reports on the utilization of silica xerogel doped with Cu and Ag [16] nanoparticles were also cited in the literature towards the oxidation of benzene; these nanocomposites catalyzed benzene directly to $H_2O$ and $CO_2$.

In the present work, direct in situ synthesis of silver nanoparticles in silica aerogel matrix has been carried out. A cost-effective and an easy-to-handle sub-critical drying method was adopted [17]. The stabilization of silver nanoparticles aided by the aerogel matrix has motivated the present work in evaluating their catalytic performance towards the selective oxidation of benzene.

## 2 Experimental

### 2.1 Material Preparation

Monolithic silica aerogel was prepared by ambient sub-critical drying method. A sol composition of TEOS:ethanol:acidified water (0.001 N nitric acid) in the molar ratio of 1:4:16 has been chosen. In a typical experiment, to obtain 10 g of silica 34.72 g of TEOS was weighed out and homogenized using 30.71 g of EtOH. Hydrolysis of the sol was brought out using 48 g of acidified water. Silver nanocomposites with 1, 5, 10 and 25 wt.% of silver were prepared in the present work. Silver nitrate of 0.157, 0.78, 1.57 and 3.937 g was added to the acidified water so as to prepare the desired silver wt.% of the nanocomposites. During the hydrolysis step, the silver sols were kept closed with a black cover so as to prevent the aerial reduction of silver ions to silver.

Sub-critical drying method was then adopted to obtain monolithic silver/silica aerogel nanocomposites, which involved the following steps. The as-gelled samples were exchanged with 1:1 ethanol: water mixture, washing was done 5 times in 24 h. Exchange with absolute ethanol was then performed; five times in 24 h to obtain gels in an alcohol medium. Alcohol exchanged gels were then aged in TEOS solution (1:1 ratio of TEOS:ethanol) for 24 h. The as-aged silica gels were then solvent exchanged with ethanol for five times in 24 h. Drying of the gels was done initially at 50 °C for 24 h, followed by drying at 70 °C for 24 h. Final drying was carried out at 120 °C for 24 h resulting in the monolithic silver-silica aerogel (SSA) nanocomposite. These samples were then heat-treated at 300 °C in $H_2$ atmosphere at the heating rate of 3 °C $min^{-1}$ with a soaking period of 3 h. These samples will be hereafter labeled as 1%Ag, 5%Ag, 10%Ag and 25%Ag, respectively throughout this article.

### 2.2 Physico-chemical Characterization

XRD patterns were recorded using Phillips PWD 1830 model X-ray diffractometer with CuKα radiation. For microstructural (TEM) studies, the gel samples were ground and dispersed in acetone. A few drops were placed onto a carbon-coated copper grid. After the evaporation of solvent, the copper grid was mounted in a Phillips EM 430 T model transmission electron microscope for microstructural and selected area electron diffraction investigations. The textural properties of the silica aerogel were determined by nitrogen sorption technique at −196 °C, using Quantasorb surface area analyzer. Initially the aerogel was degassed at 573 K for 3 h in vacuum and the adsorption–desorption isotherms were obtained at 77 K. The specific surface area was calculated using Brunauer–Emmett–Teller (BET) method and the pore size distribution (PSD) was estimated by Barrett–Joyner–Halenda (BJH) method as per the ASTM standard D4641/87. X-ray photoelectron spectroscopic (XPS) analysis was done using Kratos axis ESCA spectrometer with a hemispherical analyzer operating at 20 eV. An AlKα X-ray source (hυ = 1486.6 eV) was used as the exciting radiation and the pressure inside the experimental chamber was maintained at ca.$10^{-9}$ Torr.

### 2.3 Catalytic Testing of SSA Nanocomposites

Powdered SSA nanocomposite samples of 1%Ag, 5%Ag, 10%Ag and 25%Ag were used for the catalytic study. The oxidation reactions were carried out in a fixed bed down flow reactor at atmospheric pressure in the temperature range of 200–450 °C at the intervals of 50 °C. The temperature of the reactor was controlled and measured by a thermocouple positioned along the outside wall of the glass reactor. The reactor was charged with 0.5 g of the catalyst material diluted with ceramic beads. The flow rate of the reactant was controlled by a syringe infusion pump. The flow rate of benzene was varied from 1.5 mL/h to 2.5 mL/h and the flow rate of air was maintained at 150 mL/min. After a pre-treatment of the material at 500 °C in air for 2 h, the reactants were introduced into the reactor. The influence of temperature was studied for benzene oxidation over all the SSA nanocomposite (1%Ag, 5%Ag, 10%Ag and 25%Ag) samples. The reaction products were immediately quenched and analyzed for the oxidation products and the reactants. The products collected at the bottom of the reactor were analyzed by Clarus500 gas chromatograph

(Perkin Elmer) using elite 5 ms, 25 mts capillary column further the products were confirmed by GC-MS technique.

## 3 Results and Discussion

### 3.1 Microstructural Evaluation

Figure 1 shows the powder X-ray diffraction patterns of silica aerogel, 1%, 5% and 25%Ag samples heat-treated at 300 °C in $H_2$ atmosphere. In all the patterns, the presence of amorphous silica is evidenced by diffused background intensity. As the silver content was increased, XRD peaks corresponding to crystalline silver started appearing in the XRD patterns; increased peak intensity with increasing concentration of silver. The XRD patterns were indexed to the fcc unit cell of silver with $a$ = 4.08 (±0.004) nm.

The bright field TEM microstructure of 1%Ag sample is shown in Fig. 2a. The microstructure revealed the presence of well-dispersed, spherical silver particles in this sample. The particle size histogram made for this sample using the above microstructure is shown in Fig. 2a′. Approximately 70 particles were sampled from several areas in the TEM images and were used to obtain the particle size histogram. The analysis showed that most of the silver particle diameter was in the range of 6–8 nm.

The bright field TEM image of 5%Ag sample is shown in Fig. 2b. Spherical silver particles can be observed for this SSA nanocomposite also. The particle size histogram was generated from the TEM microstructure as shown in Fig. 2b′. From the histogram it was observed that the diameter of silver particles is in the range of 10–15 nm. Figure 2c shows the dark field TEM microstructure of 25%Ag sample. The silver particles were dispersed in the aerogel matrix with non-spherical particle morphology, as

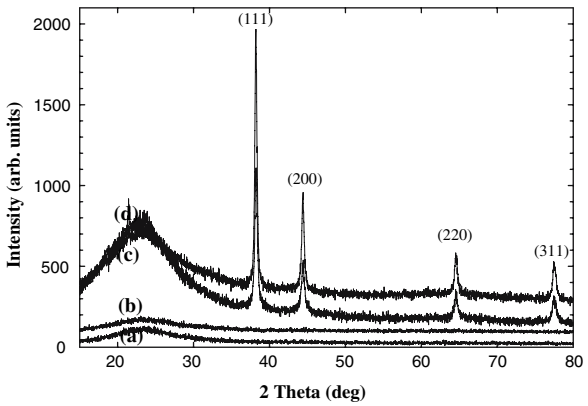


**Fig. 1** X-ray diffraction patterns of (**a**) silica aerogel and (**b**) 1%Ag samples showing amorphous pattern. The XRD patterns of (**c**) 5%Ag and (**d**) 25%Ag samples shows the peaks corresponding to the fcc metallic silver phase

can be seen in the microstructure. The particle size histogram was generated for this sample and is shown in Fig. 2c′. From the histogram analysis, it was observed that the silver particle diameter is in the range of 25–100 nm.

In 25%Ag sample silver particles were segregated from the silica aerogel matrix, Fig. 3. The nature of crystallinity of silver nanoparticles was evaluated using selected area electron diffraction studies. A single crystalline silver (Fig. 4a) from 25%Ag sample was selected and diffracted along the [011] zone axis of the fcc unit cell. From the diffraction pattern (Fig. 4b) the lattice parameter of fcc silver was calculated. The calculated lattice parameter value was comparable with the ASTM bulk silver lattice parameter values.

### 3.2 Textural Characterization

Nitrogen adsorption measurement was done to determine the surface area and pore structural characteristics of SSA nanocomposites. The isotherm branches in both the adsorption and desorption cycle were measured for silica aerogel and 1wt.%Ag sample in the partial pressure ($p/p_0$) range of 0.05–1.0, Fig. 5a and b. Figure 5a′ and b′ shows the average pore size distribution of the above said samples. From the shape of the isotherms, it can be seen that the material exhibited type IV isotherm in both these samples. With increasing silver concentration, the specific surface area decreased from 845 $m^2\ g^{-1}$ to 307 $m^2\ g^{-1}$ as shown in Table 1. This concomitant decrease in surface area with increasing silver concentration showed that fine silver particles crystallized within the pores of the aerogel matrix as shown in Fig. 6.

H2 type of hysteresis was observed in these samples that showed the existence of silica particles of non-uniform shape and size interconnected by cylindrical pores [18]. The average pore size distribution was ~5 nm for silica aerogel and ~6 nm for 1%Ag SSA sample (Fig. 5a′, b′). This was evaluated using the BJH analysis. The total pore volume was found in the range of 0.4 $cm^3\ g^{-1}$ to 0.87 $cm^3\ g^{-1}$ for the aerogel and SSA nanocomposite samples. The largest total pore volume (0.87 $cm^3\ g^{-1}$) was obtained for 1%Ag sample and it subsequently decreased for 5, 10 and 25%Ag samples. This characteristic was attributed to the partial replacement of silicon by silver atom in the silica framework and the associated vacancy created for the charge compensation. With increasing silver concentration, the silver atoms get crystallized in the pores of the aerogel matrix. Thus crystallization of more silver particles reduced the total pore volume of the aerogel matrix for 5, 10 and 25%Ag samples.

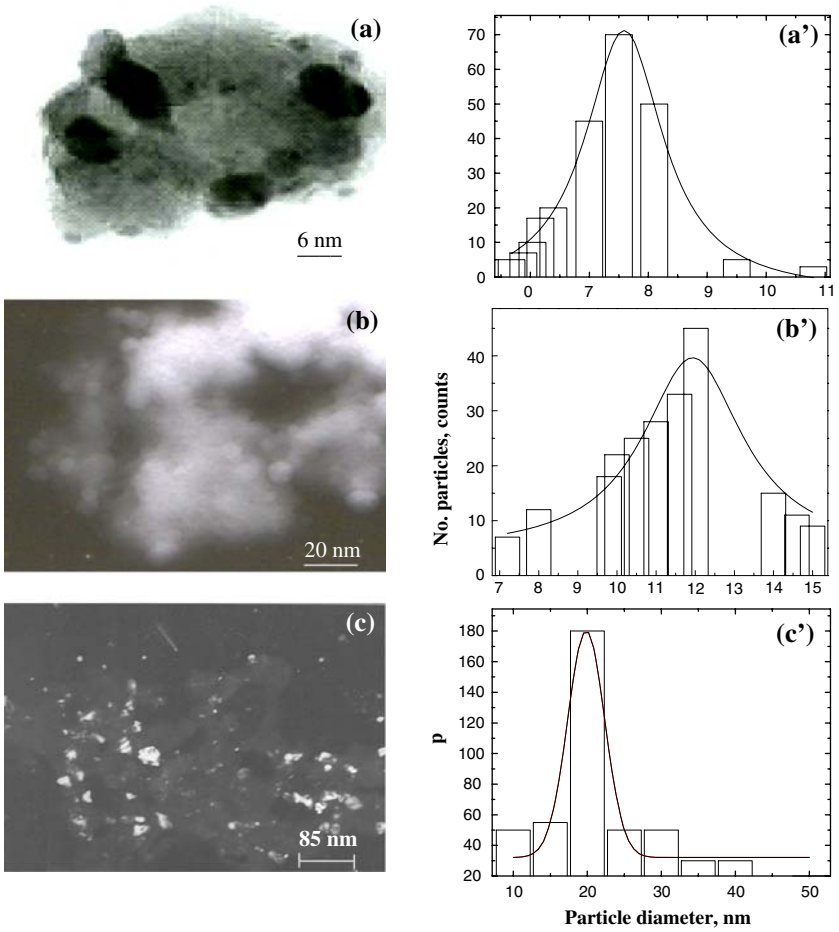


**Fig. 2** (**a**) Bright field TEM image of 1%Ag sample and its (**a′**) particle size histogram. (**b**) Bright field TEM image of 5%Ag sample and its (**b′**) particle size histogram. (**c**) Dark field TEM image of 25%Ag sample and its (**c′**) particle size histogram

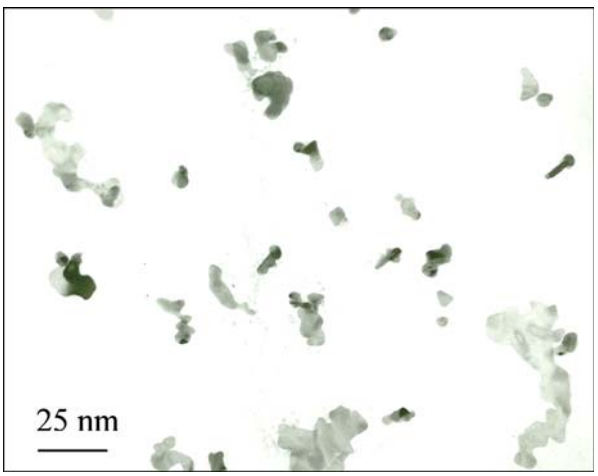


**Fig. 3** Bright field TEM image of 25%Ag sample showing segregated single crystalline silver

### 3.3 Catalytic Performance

The catalytic activity of the nanocomposites towards the oxidation of benzene was evaluated in the temperature range of 200–400 °C at 50 °C interval. The influence of temperature on benzene oxidation was studied over all the 1, 5, 10 and 25%Ag SSA nanocomposite samples. The aerogel materials without silver were also tested for its catalytic activity. It did not show any conversion under similar reactions conditions maintained for the SSA nanocomposites. Among all the samples, 1%Ag sample exhibited high conversion rate. The % conversion of benzene increases as the temperature increases for all the silver loaded catalysts. Beyond 400 °C, the % conversion notably decreased, which might be due to the blocking of pores as well the active sites by the carbonaceous material appeared during the course of reaction. In all the cases, phenol selectivity was found not less than 90%. Thus the effect of temperature variation on phenol selectivity was performed only with the 1%Ag sample and is shown in Fig. 7.

The selectivity of phenol decreased as the temperature was raised above 300 °C. The catalytic activity in general depends strongly on the size and dispersion of the metallic nanoparticles in the porous matrix. It is also known that aggregation of nanoparticles occurs with increasing heat-treatment temperature. An increase in silver particle size and its associated aggregation of silver nanoparticles might be the reason for the lowered selectivity of SSA nanocomposites with increasing temperature. Thus at lower

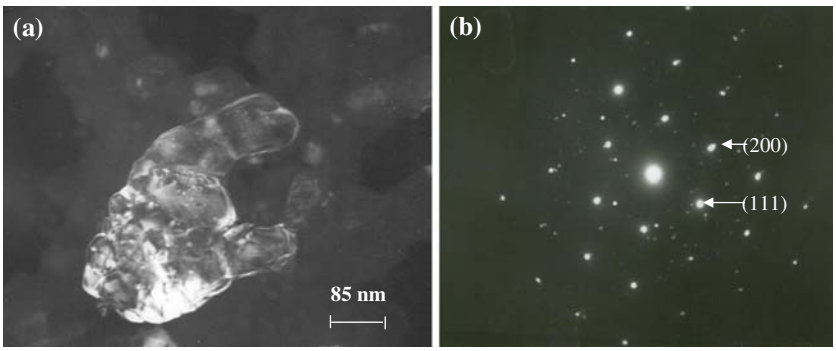


**Fig. 4** (**a**) Dark field TEM image of 25%Ag sample showing dendritic single crystal silver; small silver particles are found on the surface of the single crystal silver. (**b**) Diffraction pattern taken from the microstructure along the [011] zone axis of the fcc crystal structure

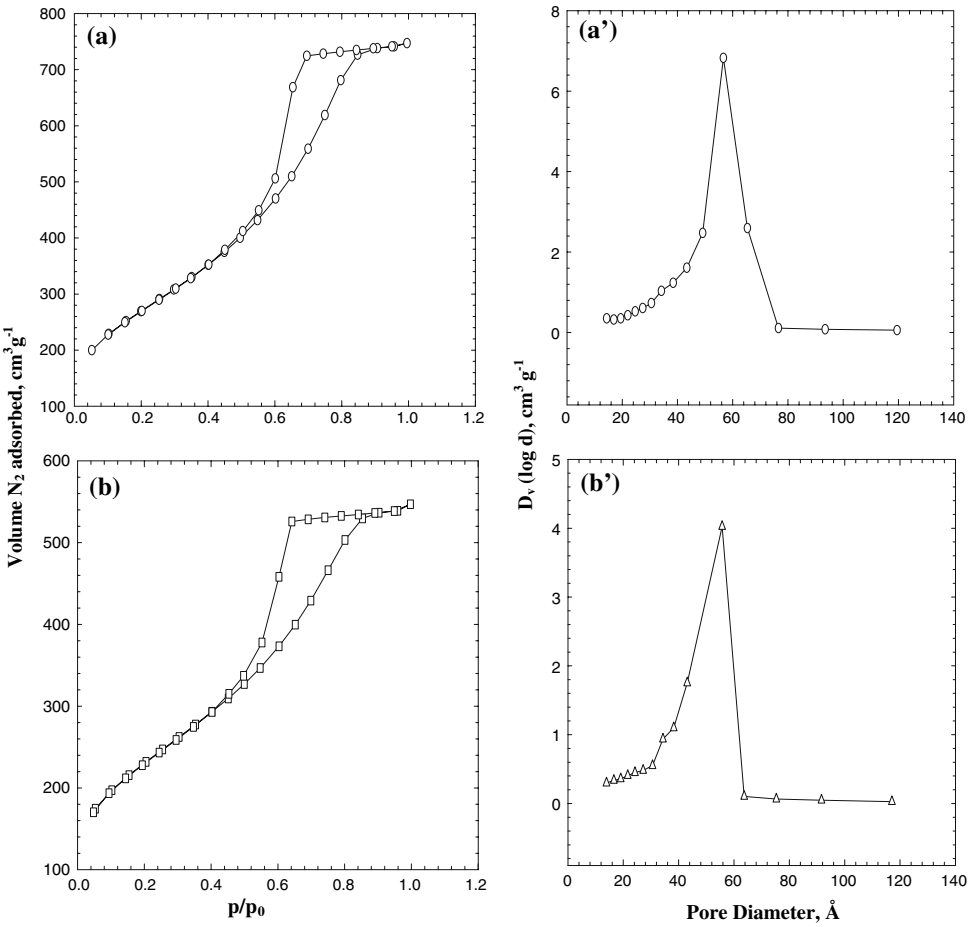


**Fig. 5** Nitrogen adsorption/desorption isotherms of (**a**) silica aerogel and (**b**) 1%Ag sample, degassed at 200 °C. The pore size distribution of (**a′**) silica aerogel and (**b′**) 1%Ag sample shows the similar pore size distribution in both the samples

**Table 1** Textural properties of silica and SSA nanocomposites degassed at 200 °C

| Sample | Specific surface area ($m^2\ g^{-1}$) | Total pore volume ($cm^3\ g^{-1}$) |
|---|---|---|
| Silica aerogel | 845 | 0.50 |
| 1%Ag nanocomposite | 603 | 0.87 |
| 5%Ag nanocomposite | 519 | 0.76 |
| 10%Ag nanocomposite | 437 | 0.52 |
| 25%Ag nanocomposite | 307 | 0.37 |

temperature, the selectivity was maximum for 1%Ag sample, which had a smaller particle diameter and a narrow particle size distribution. The total pore volume was also found maximum for this sample. The lowered selectivity for the 25%Ag sample can then be assigned to the larger and a wider particle size distribution when compared to the 1%Ag sample. In all the samples tested, with increasing temperature the percentage conversion also increased. In general, an increase in the temperature will enhance the rate of the chemical reaction thus increasing the percentage conversion.

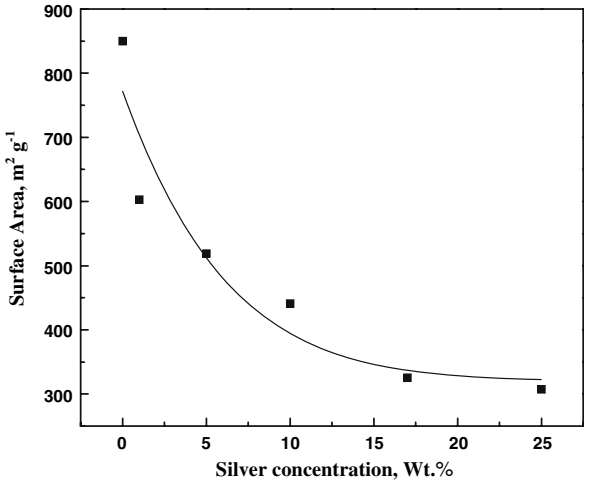


**Fig. 6** The variation of surface area with increasing silver concentration showing the crystallization of silver in the aerogel matrix

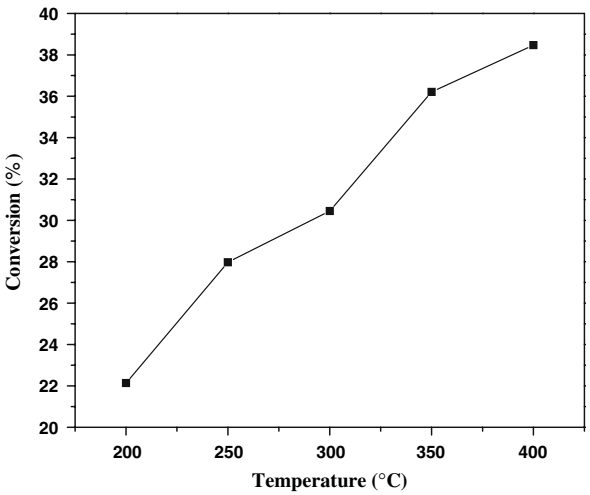


**Fig. 7** The effect of temperature on the percentage conversion to phenol for the 1%Ag sample

Various mechanisms have been proposed to model the oxidation of benzene proceeding through stable and radical intermediates [19–21]. The XPS analysis was performed with the 25%Ag sample before and after the catalytic tests to determine the changes in the oxidation states of silver species. The deconvoluted Ag 3d level XPS spectrum of 25%Ag sample is shown in Fig. 8. Three different forms of silver species can be observed from the XPS spectrum with binding energy values of 368.2, 367.8 and 367.4 eV. This was assigned to the silver species of $Ag^0$, $Ag^{2+}$and $Ag^+$, respectively [22]. The ratio of these silver species was 55:14:31 and 54:34:12 before and after the catalytic oxidation studies. The concentration of $Ag^{2+}$ species increased after the oxidation reaction with a concomitant decrease in the amount of $Ag^0$ and $Ag^+$ species.

The possible pathway for the oxidation of benzene over silver aerogels is postulated by assuming $Ag_2O$, AgO and

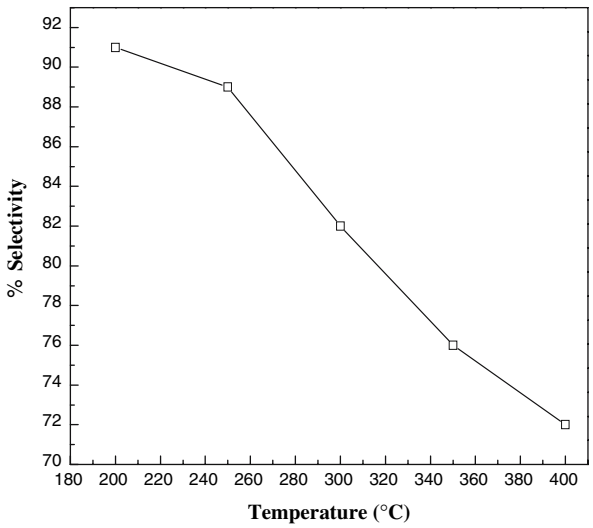


**Fig. 8** The effect of temperature on the percentage selectivity of benzene for the 1%Ag sample

Ag species to be the active centers. Though the exact structure of the active centre is not explained, it is proposed that it might be a metal-oxo species of $Ag^{2+}$ as confirmed by the recent XPS studies. The possibility of participation of the silver species in the oxidation of benzene was also confirmed from the products obtained by GC-Mass spectrometry.

The XPS analysis of 25%Ag sample tested after the catalytic oxidation reaction also possessed various forms of carbon. The binding energies of carbon were 284.7, 286.2 and 287.9 eV, respectively, as shown in Fig. 9. The presence of various forms of carbon was due to the deposition of coke in the pores of aerogel matrix at high temperature blocking the active sites of the catalyst. This also decreased the activity of the 25%Ag catalyst towards the selectivity to phenol, when compared to the 1%Ag sample. The use of silver catalyst towards the oxidation of benzene has been cited scarcely in the literature [23]. Supercritical drying

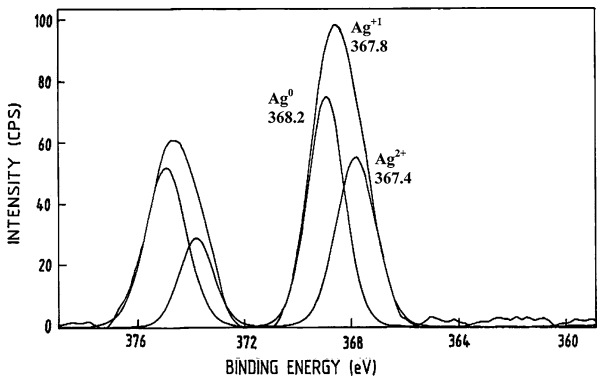


**Fig. 9** The deconvoluted XPS spectra of Ag 3d level in 25%Ag sample before (*dotted line*) and after (*solid line*) the catalytic oxidation reaction of benzene

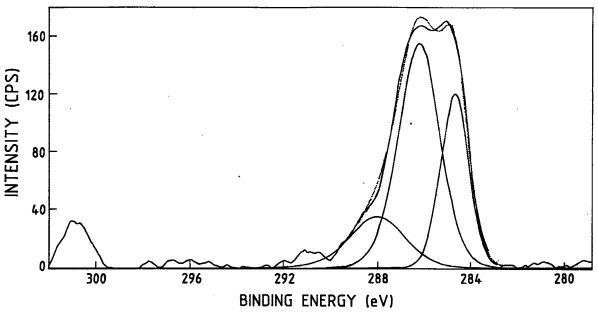


**Fig. 10** The deconvoluted XPS spectra of carbon 1s level in 25%Ag sample, taken after the catalytic oxidation of benzene at 300 °C

technique has also been adopted, where benzene was reported to be fully oxidized to $CO_2$ and water instead of phenol [24]. Thus, the present methodology is advantageous in oxidizing benzene selectively to phenol. Further, experimental optimization of the catalytic oxidation needs to be done towards the full utilization of the present SSA nanocomposite prepared by the sub-critical drying method (Fig. 10).

## 4 Conclusion

In summary, homogeneous and well-dispersed silver nanoparticles were prepared in the silica aerogel matrix using sub-critical drying method. The effect of the aerogel matrix in the stabilization of silver nanoparticles was confirmed by various physico-chemical characterizations. The efficacy of the SSA nanocomposite towards the selective oxidation of benzene was proved. The catalytic oxidation was effective for benzene oxidation, with the highest selectivity observed with 1%Ag sample. The selectivity to phenol was not less than 90% for all the tested SSA nanocomposite samples. The maximum selectivity observed with the 1%Ag sample was attributed to the narrow silver particle size distribution within the aerogel matrix. With larger particle size of silver, as in the case of 25%Ag, the selectivity of the reaction was less. This has been attributed to the larger and wider silver particle size distribution observed in this sample.

**Acknowledgements** The authors are thankful to the organization, DMRL for extending its technical support for carrying out this work. Support extended by Shri. K. Prasad of Electron microscopy Group (DMRL) is highly acknowledged.

## References

1. Pajonk GM (1991) Appl Catal 72:217
2. Teichner SJ (1991) Chem Technol 21:372
3. Fricke J, Emmerling A (1992) Chemistry, spectroscopy and applications of sol–gel glasses, structure and bonding, vol 77. Springer-Verlag, p 37
4. Hair LM, Owens L, Tillotson T, Fröba M, Wong J, Thomas GJ, Medlin DL (1995) J Non-Cryst Solids 186:168
5. Schwertfeger F, Frank D, Schmidt M (1998) J Non-Cryst Solids 225:24
6. Motonobu G, Yoshinori M, Tsutomu H (1996) Micropor Mater 7:41
7. Blanchard F, Reymond JP, Pommier B, Teichner SJ (1982) J Mol Catal 17:171
8. Shu-ichi N (2002) AIST Today 2:15
9. Hyunwoong P, Wonyong C (2005) Catal Today 101:291
10. Ken-ichi S, Hiroya A, Tatsuya K, Yoshie K (2004) Appl Catal A 269:75
11. Kuznetsovaa NI, Kuznetsova LI, Likholobov VA, Pez GP (2005) Catal Today 99:193
12. Niazyan OM, Mantashuan AA, Nalbandyan AB (1968) Armenian Chem J 21(3):266
13. Umemura S, Kitoh R, Uda T (1982) USA Patent 433:871
14. Zhang W, Wang J, Tanev PT, Pinnavaia TJ (1996) Chem Commun 979
15. Zhang J, Tang Y, Li G, Hu C (2005) Appl Catal A 278:251
16. Stéphanie L, Caroline C, Gaigneaux EM, Jean-Paul P, Benoît H (2007) Catal Commun 1244
17. Balkis Ameen K, Rajasekharan T, Rajasekharan MV (2006) J Non-Cryst Solids 352:737
18. Walker GS, Williams E, Bhattacharya AK (1997) J Mater Sci 32:5583
19. Emdee JL, Brezinsky K, Glassman I (1992) J Phys Chem 96:2151
20. Zhang HY, McKinnon JT (1995) Combust Sci Technol 107:261
21. Tan Y, Frank P (1996) Proc Combust Inst 26:677
22. Hammond JS, Gaarenstroom SW, Winograd N (1975) Anal Chem 47:2194
23. Lambert S, Cellier C, Grange P, Pirard JP, Heinrichs B (2004) J Catal 221:335
24. Stéphanie L, Caroline C, Paul G, Jean-Paul P, Benoît H (2004) J Catal 221:335